Appl Nanosci (2013) 3:535–542
DOI 10.1007/s13204-012-0162-0

ORIGINAL ARTICLE

$Zn_3(VO_4)_2$ prepared by magnetron sputtering: microstructure and optical property

Surayya Mukhtar · Chongwen Zou · Wei Gao

Received: 14 August 2012 / Accepted: 25 September 2012 / Published online: 20 October 2012

Abstract Zinc vanadium oxide $Zn_3(VO_4)_2$ has been prepared by means of DC magnetron sputtering and subsequent post heat treatment. The samples were synthesized via two routes: dual-target co-sputtering of ZnO and V_2O_5 or the ordinal deposition of V_2O_5 and ZnO thin layers. The obtained precursors were then annealed in oxygen atmosphere from 500 to 550 °C to form the $Zn_3(VO_4)_2$ compound. Morphology and composition of the samples have been investigated by means of scanning electron microscope and energy-dispersive X-ray spectroscopy. X-ray diffraction pattern shows the presence of α-$Zn_3(VO_4)_2$, ZnO and vanadium oxide in the annealed ZnO–V_2O_5 samples. Pure V_2O_5 with two distinct phases, β and γ phases, is found for the samples annealed at 500 °C. Room temperature photoluminescence properties have been studied, and the annealed samples exhibit excellent light emission in the visible region centred at 528 nm from $Zn_3(VO_4)_2$ compound. The light emission from $Zn_3(VO_4)_2$ is discussed based on charge transfer and Frank–Condon principles.

S. Mukhtar (✉) · C. Zou · W. Gao
Department of Chemical and Materials Engineering,
The University of Auckland, PB 92019,
Auckland 1142, New Zealand
e-mail: smuk019@aucklanduni.ac.nz

C. Zou
e-mail: czou@ustc.edu.cn

W. Gao
e-mail: w.gao@auckland.ac.nz

C. Zou
National Synchrotron Radiation Laboratory,
University of Science and Technology of China,
Hefei 230026, China

Keywords Zinc oxide · Vanadium pentoxide · Magnetron sputtering · Photoluminescence

Introduction

Vanadium pentoxide (V_2O_5) is the most stable oxide in the vanadium oxide system, which has an indirect bandgap of about 2.2–2.4 eV energy. Owing to its unique layered structure, V_2O_5 shows interesting optical and electronic properties, thereby attracting attention for the research and applications in diverse areas such as chemical sensing, multi-coloured photochromism, cathode material in batteries and catalysis (Legrouri 1993; Moshfegh 1991; Schoiswohl et al. 2004; Talledo et al. 2003; Fei et al. 2008; Hu and Zhong 2005; Stoyanov et al. 2006). Recently, research indicated that V_2O_5 has shown light emission in visible region; and the photoluminescence (PL) intensity can be improved by heat treatment (Wang et al. 2007). However, owing to the relatively weak PL intensity, V_2O_5 has not been considered for the light emission applications.

It has been observed that the combination of V_2O_5 with other transition metal oxides improves the electronic, optical and catalytic characteristics of the composite system (Zou et al.2009a, 2010a, b; Liu et al. 2007; Stoyanov et al. 2006). Similarly, vanadates such as $Mg_3(VO_4)_2$, $LiZn(VO_4)_2$ and $NaCaVO_4$ show good luminescence properties. Upon further doping with rare earth element ions such as Eu^{3+} ions, vanadate complexes such as $Ba_3V_2O_8$ and $Ca_3Sr_3(VO_4)_4$ show enhanced fluorescence light emission (Chen et al. 2010; Choi et al. 2009). In fact, these compounds generally have VO_4^{3-} group in which V^{5+} ion is surrounded by four O^{2-} ions in tetrahedral symmetry. Upon photoexcitation, the charge transfer from oxygen to vanadium ion is pronounced. Accordingly, efficient

energy transfers from the vanadate ions to luminescent centres take place easily, making these compounds attractive candidates for luminescent applications.

As a typical vanadate, $Zn_3(VO_4)_2$ has fascinating microstructure with high porosity. The lattice is assembled from layers of Zn octahedral connected by tetrahedral vanadate groups (Hoyos et al. 2001; Umemura et al. 2006). It has three polymorphs; α, β and γ—α-$Zn_3(VO_4)_2$ is the stable room temperature phase, whereas β and γ are the non-quenchable high-temperature phases (Hng and Knowles 1999). Till now, few studies have reported the crystal structure, synthesis and characterization of $Zn_3(VO_4)_2$. In a recent article, two methods have been described for the synthesis of $Zn_3(VO_4)_2$: hydrothermal and citrate–gel combustion method (Pitale et al. 2012). In another study, $Zn_3(VO_4)_2$ has been prepared by hydrothermal method from $Zn_3(OH)_2V_2O_7.nH_2O$ as the starting material.(Ni et al. 2010) These reports describe strong photoluminescence emission in the visible region from $Zn_3(VO_4)_2$ compound. However, the origination of the visible light emission is still not fully understood, and the relationship between the microstructure and the optical property needs detailed investigation.

In this article, we report the preparation of $Zn_3(VO_4)_2$ by means of magnetron sputtering method with two different deposition routes and subsequent heat treatment. The influencing factors, such as annealing temperature and deposition parameters, on the microstructure and luminescence properties of $Zn_3(VO_4)_2$ have been systematically studied. Strong photoluminescence in visible region has been observed, which demonstrates that $Zn_3(VO_4)_2$ compound can be a potential material for light emission applications.

Experimental details

Two types of samples, A and B, were prepared by DC magnetron sputtering on glass substrates in Ar atmosphere. The glass substrate was rinsed in alcohol, cleaned in ultrasonic bath for 10 min and then blown dried using hot air. After introduced into the sputter chamber, Ar plasma produced by RF was used to further clean the glass substrate surface for 1 h before deposition. Ar was used as the working gas. The background pressure of the sputter chamber was 2.67×10^{-4} Pa. The working gas pressure was 1.33 Pa with a flow rate of 1.67×10^{-7} m^3/s. During the deposition, the substrates were rotated with the speed of 3 rpm.

Sample A was prepared by dual-target co-sputtering of pure ZnO (99.9 %) and V_2O_5 (99.9 %) at room temperature. In the sputtering chamber, ZnO and V_2O_5 targets were installed at 180° (parallel) to each other, and thus co-sputtering experiment can be conducted. The deposition time was 4 h with a DC current of 0.25 A. After deposition, the samples were annealed in a tube furnace at 500 and 550 °C in oxygen atmosphere with a flow rate of 3.3×10^{-6} m^3/s. The crystallization and optical properties of V_2O_5 are known to be sensitive to annealing temperature. Therefore, temperature of furnace was carefully calibrated with thermocouple before annealing.

Sample B was prepared involving four steps: (1) deposition of V_2O_5 by sputter for 4 h with DC current of 0.35 A on glass substrate at room temperature; (2) subsequent annealing the V_2O_5/glass sample in oxygen atmosphere at 500 °C for 1 h to form the V_2O_5 crystals; (3) sputtered ZnO with DC current of 0.25 A onto the annealed V_2O_5/glass for 40 min at room temperature; and (4) after ZnO deposition, the ZnO/V_2O_5/glass samples were again annealed at 500 °C in oxygen atmosphere for 1 h at the same flow rate as for sample A.

Crystal structures of the obtained samples were investigated by X-ray Diffraction (XRD) with Cu Kα radiation (Bruker D2). Microstructures and compositions of the products were examined by means of Philips XL-30S scanning electron microscope (SEM) equipped with energy-dispersive x-ray spectroscopy (EDS). For EDS analysis, beam line with spot size 4 and 20 kV voltage has been used which gives penetration depth of $\sim$1 μm. The room temperature photoluminescence (PL) test was performed by a He–Cd laser ($\lambda = 325$ nm) to investigate the light emission properties of the samples.

Results and discussion

To study the crystalline structure and phase changes in sample A before and after heat treatment, XRD has been performed as shown in Fig. 1. The sample without heat treatment shows no diffraction peaks in the pattern, indicating an amorphous structure (Fig. 1a). It is consistent with the previous report that the pure V_2O_5 prepared by sputter at room temperature always shows amorphous structure at room temperature (Zou et al. 2009a, b). The obtained XRD result indicates that the simultaneous sputtering from both targets does not favour the ZnO crystallization, which is perhaps due to the disruption of crystal structure of ZnO by the unbalanced stoichiometry of V_2O_5 and ZnO. Another possible explanation is ascribed to the presence of high content of vanadium in the film which leads to the distortion of ZnO crystal lattice through incorporation of V atoms at the Zn points (Wang et al. 2010).

Upon heating to 500 °C, diffraction peaks indexed as ZnO and α-$Zn_3(VO_4)_2$ are noted (Fig. 1b), implying that weak crystallization process has started because of the

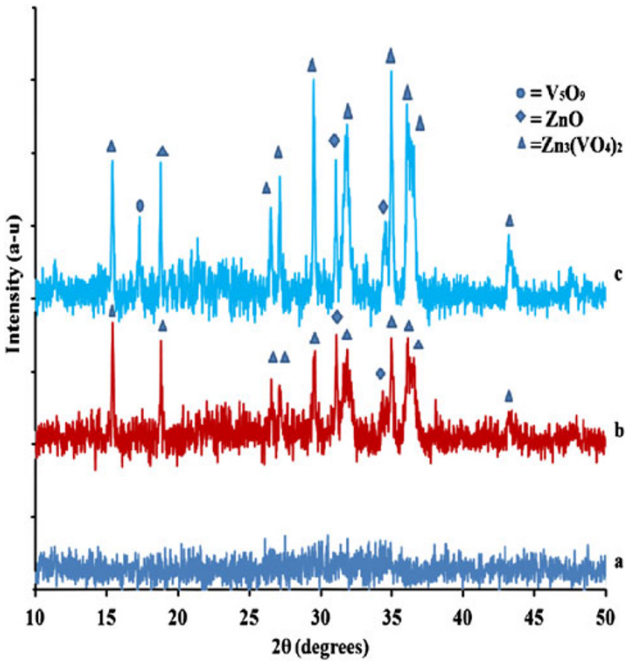

Fig. 1 XRD pattern of sample A: (*a*) without heat treatment; (*b, c*) annealed at 500 and 550 °C in oxygen atmosphere

surface diffusion process. At the annealing temperature of 550 °C, three major phases appeared in the XRD pattern, α-$Zn_3(VO_4)_2$, V_5O_9 and ZnO (Fig. 1c). α-$Zn_3(VO_4)_2$ is a low temperature polymorph, which has the orthorhombic crystalline structure with a = 0.6088, b = 1.1498 and c = 0.8280 nm according to JCPDS No. 73–1300.

Microstructure and morphology of the sample A before and after heat treatments at 500 and 550 °C have been investigated by SEM as shown in Fig. 2. The total thickness of the film measured by the SEM cross section is ~950 nm. It is observed that the film without heat treatment consist of nanoparticles separated by void regions (Fig. 2a). Changes in surface morphology are noted by annealing the sample at different temperatures. At 500 °C, the amorphous nanoparticles started to agglomerate and form small crystals as viewed in Fig. 2b. The cross section shows thick and dense film after heat treatment as shown in the inset of Fig. 2b. After an annealing at 550 °C, some big crystals appeared on the surface (Fig. 2c). The underneath bush-like structures can be seen through the voids between these crystals.

To further investigate the composition of the sample annealed at 500 °C, EDS was performed. Vanadium and zinc elements are clearly observed from the spectrum as shown in Fig. 2d. The Si and Au peaks come from the glass substrate and coating of sample respectively. The atomic ratio of Zn:V:O is 50:15:35, while the atomic ratio of Zn:V:O should be 23:15:62 according to the molecular formula of $Zn_3(VO_4)_2$. Thus, the EDS result shows the presence of Zn interstitials or oxygen vacancies, if we assume that all ZnO and V_2O_5 have been transformed to a compound $Zn_3(VO_4)_2$. However, XRD results indicate the presence of ZnO and V_5O_9 in the annealed sample at 550 °C. This confirms that the ZnO and V_2O_5 are not fully mingled at temperature ≤550 °C. By combining the EDS and XRD results, two possible explanations for incomplete formation of $Zn_3(VO_4)_2$ are proposed: first, the annealing temperature is not high enough to provide the required activation energy for the formation of $Zn_3(VO_4)_2$ as mentioned in the ZnO–V_2O_5 phase diagram (Kurzawa et al. 2001). The second reason lies on the fact that Zn, V and O atoms are not stoichiometrically distributed in the film as the sample is prepared by the dual target co-sputtering, thus the atomic ratio of Zn and O atoms does not match with the composition of $Zn_3(VO_4)_2$. Zn is found in excess whereas O is deficient as indicated by EDS result. Thus, it is understandable that Zn interstitials have combined with O atoms to form ZnO, whereas V and O atoms in combination formed low oxidation state vanadium oxide, i.e., V_5O_9 in the samples annealed at 550 °C. As a result, the V:O ratio has been reduced from 2.5 to 1.8 during the phase change from V_2O_5 to V_5O_9 because of the deficiency of O atoms in the film.

The XRD pattern of pure V_2O_5/glass sample after heat treatment at 500–550 °C in oxygen atmosphere give rise to two diffraction peaks associated with strong β-V_2O_5 with the preferred (200) orientation and γ-V_2O_5 as observed in Fig. 3a–b. The intensity of both β-V_2O_5 and γ-V_2O_5 phases increases with increasing temperature, which indicates the temperature sensitive crystallization. α-V_2O_5 has not been observed at any stage as reported previously for pure V_2O_5 annealed at 550 °C (Zou et al. 2009b).

To investigate the crystal structure and phases formed in the V_2O_5–ZnO binary system, XRD was performed on sample B before and after heat treatment. Fig. 3c shows the XRD pattern of the sample without heat treatment after ZnO thin layer deposition. Two major peaks have been noted in the pattern; β-V_2O_5 at 12.2° and ZnO at 34.4° indicating that both V_2O_5 and ZnO maintains the separate phase and requires high energy to form zinc vanadium oxide compounds. The sputtering process at room temperature does not provide this energy, thus the post-deposition heat treatment at critical temperature is required to provide enough kinetic energy for the solid phase reaction. It is clear that after heat treatment at 500 °C in oxygen atmosphere, sample B shows α-$Zn_3(VO_4)_2$ as major phase along with two other peaks from ZnO and γ-V_2O_5, representing that ZnO and V_2O_5 are not fully reacted to form $Zn_3(VO_4)_2$ at this temperature as shown in Fig. 3d.

The SEM images of sample B before and after heat treatment are shown in Fig. 4a–b. The sample without heat treatment after ZnO thin layer deposition shows two types

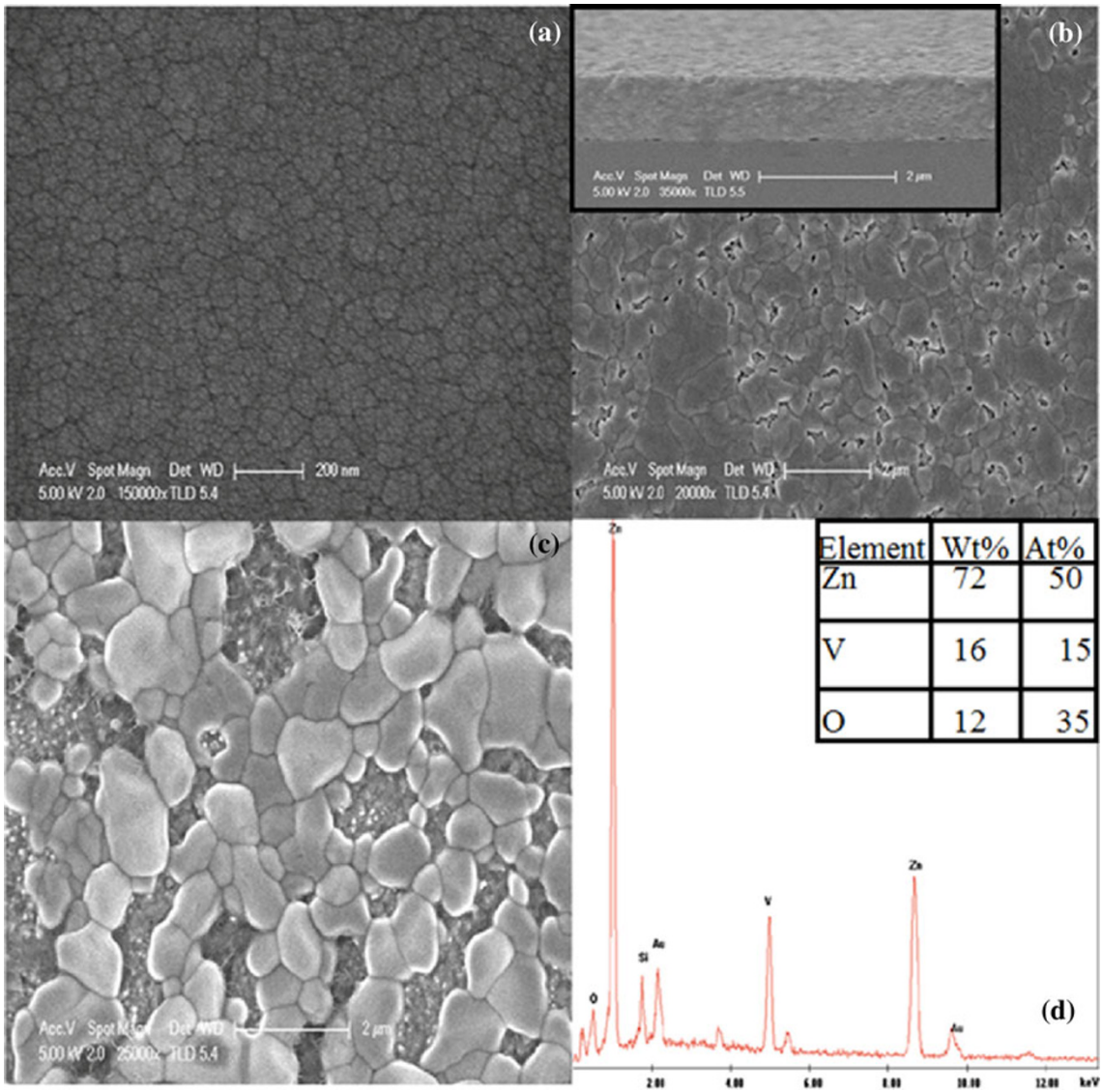

Fig. 2 SEM images of sample A: **a** without heat treatment; **b**, **c** annealed at 500 and 550 °C in oxygen atmosphere and **d** EDS pattern of sample A annealed at 500 °C

of structures: microrods with the length of several microns, and small grains. These microrods are assumed to be β-V_2O_5 according to the XRD pattern in Fig. 3a, which is consistent with the previous report that pure V_2O_5 on glass transforms to nanorods after annealing at 500 °C (Zou et al. 2009a, b). The small grains which are dispersed between the microrods might be ZnO crystals. The inset of Fig. 4b shows the cross section of the sample after heat treatment at 500 °C. It is to be noted that V_2O_5 microrods have disappeared, and the sample is quite dense, homogenous and smooth with low porosity. It can be speculated that V_2O_5 microrods are mingled with ZnO grains to form zinc vanadium oxide crystals as confirmed by XRD (Fig. 3d). By comparing the SEM images of samples A and B after 500 °C heat treatment, it can be observed that the surface morphologies seem to be similar. The EDS spectrum of annealed sample B is shown in Fig. 4c. The Zn:V:O atomic ratio is 25:24:51 which agrees quite well with the atomic ratio of $Zn_3(VO_4)_2$. Compared with sample A, sample B contains less oxygen vacancies and Zn interstitials.

He–Cd laser with the wavelength of 325 nm was used to investigate the photoluminescence (PL) properties of the samples annealed at different temperatures. Light emission could not be observed for sample A without heat treatment. Emission bands in the UV and visible region can be clearly seen from sample A after heat treatment. The PL intensity in UV and visible region increases with increasing annealing temperature from 500 to 550 °C. The UV emission band is observed at 384 nm, which corresponds to the bandgap energy of 3.23 eV for ZnO. Red shift has been

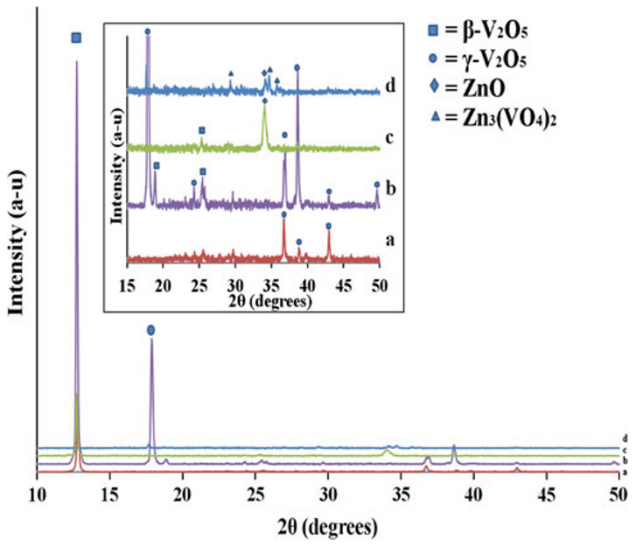

Fig. 3 XRD pattern of: (*a, b*) Pure V_2O_5 annealed at 500 and 550 °C; (*c*) sample B without heat treatment and (*d*) annealed at 500 °C in oxygen atmosphere. Inset shows the detailed XRD pattern of the same samples in the range $2\theta = 15–50^{o}$

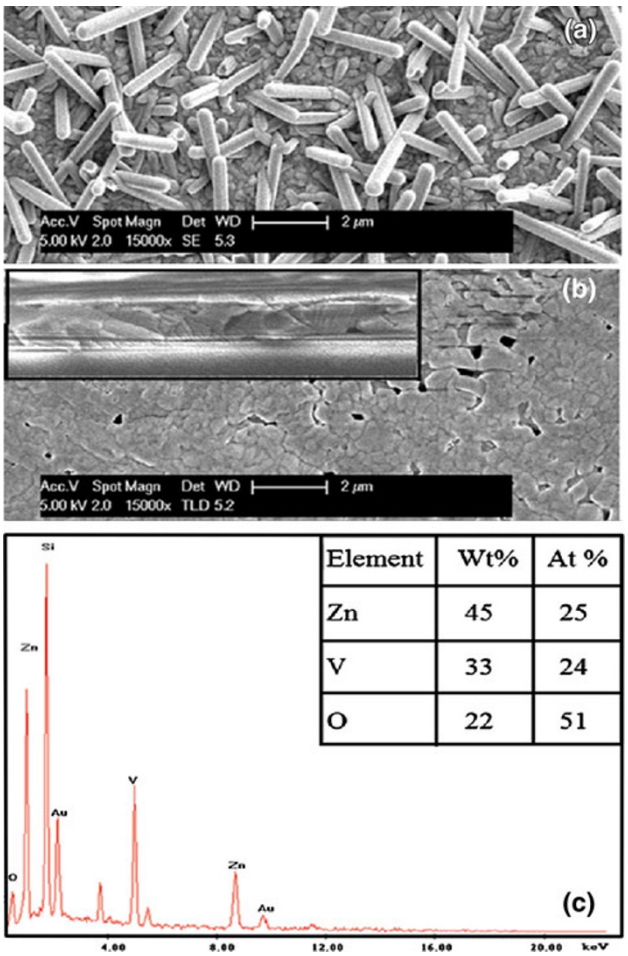

Fig. 4 SEM image of sample B: **a** without heat treatment; **b**, **c** SEM image and EDS spectra of the sample annealed at 500 °C in oxygen atmosphere

noted in the UV emission band because of the deep level transition in ZnO. It is suggested that the V ions have been partially incorporated into the ZnO lattice to form some defects, resulting in the decreased bandgap. This is the "so-called" Brustein–Moss effect induced by the external atom doping (Krithiga and Chandrasekaran 2009). The PL in the visible region centred at 528 nm shows some vibrational fine spectra, which can be attributed to the emission bands of $Zn_3(VO_4)_2$.

Weak PL has been observed from pure V_2O_5 sample annealed at 550 °C in the visible region centred at 538 nm. It corresponds to 2.34 eV, which matches the bandgap of V_2O_5. The un-annealed sample B shows weak photo-emission in the UV region which corresponds to ZnO light emission. PL in visible region has not been observed which shows that light emission from V2O5 has been suppressed by ZnO thin layer. After an annealing at 500 °C, sample B showed the highest PL emission at the same centre as sample A, i.e., at 528 nm. By comparing the XRD and PL results, we can speculate that both samples have same luminescent centre (Fig. 5).

The PL intensity of annealed sample B is double compared with sample A. Usually lattice defects such as oxygen vacancies, Zn interstitials, oxygen or Zn antisites are considered to be the sources for transitions in the visible region for ZnO. On the other hand, Zn interstitials have been considered to be highly mobile, and they can easily move to other defects to form the non-radiative defect complexes which cause the decrease in PL intensity (Muller et al. 2008). The deficiency of these defects in sample B is one of the reasons for intensive light emission in the visible region.

As the bandgap of V_2O_5 also lies in the same range as of $Zn_3(VO_4)_2$, but the un-annealed sample B has not shown any PL in the visible region, even though crystalline V_2O_5 exists. Therefore, we can speculate from the results obtained that the strong PL emission in annealed sample B is due to $Zn_3(VO_4)_2$. In this case, coupling mechanism for photoemission is not involved between the V_2O_5 and ZnO as reported earlier for V_2O_5/ZnO bilayer composite (Zou et al. 2010a, b). It indicates that coupling mechanism or resonance effect is effective only when two particles of different metal oxides come in close contact to each other to form hetrostructures. For the current situation, the un-annealed sample B does not form hetrostructures, while the annealed sample forms a new phase $Zn_3(VO_4)_2$ because of the solid solution of ZnO–V_2O_5.

For V_2O_5 doped ZnO system, the strong green band emission has been observed, whereas UV emission has

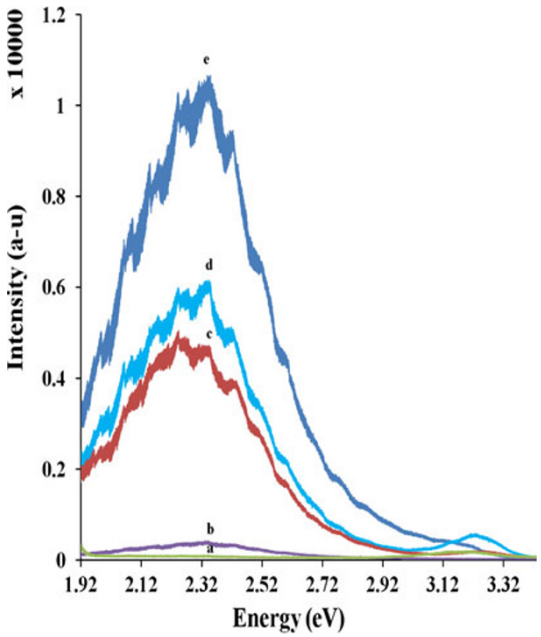

Fig. 5 PL spectra measured at room temperature (*a*) sample B without heat treatment; (*b*) pure V_2O_5 annealed at 550 °C; (*c*, *d*) sample A annealed at 500 and 550 °C and (*e*) sample B annealed at 500 °C, all in oxygen atmosphere

become weaker than pure ZnO (Kim et al. 2005). However, for the higher concentration of V_2O_5 and at a critical annealing temperature, V_2O_5 becomes soluble in ZnO, and new phase such as $Zn_3(VO_4)_2$ appears apart from ZnO and V_2O_5. High concentration of V_2O_5 introduces secondary phases in the ZnO–V_2O_5 system and gives rise to photo-emission corresponding to the new phase.

β-V_2O_5 has tetragonal or monoclinic crystal structure with lattice parameters a = 0.71140, b = 0.35718 and c = 0.62846 nm. The characteristic building unit of β-V_2O_5 consists of edge sharing of four octahedra or forming a quadruple unit. Each octrahedra consist of off-centred vanadium atom coordinated by six oxygen atoms. V_2O_5 forms layered structure with the V–O double bond, i.e., vanadyl bond of the shortest bond length of 0.1583 nm in case of β phase (Filonenko et al. 2004). Like some other transition metal oxides, V_2O_5 forms the electronic states by hybridization of V3d-O2p states. The conduction band mainly arises from the V3d bands, and it can be divided into two sub-bands: one is a broad band located at higher energy region, whereas the other one is narrow split-off band below the broad band separated by additional gaps of ~0.35 and ~0.45 eV. The valance and split-off conduction band are separated by the indirect optical bandgap of ~2.2 eV (Khyzhun et al. 2005; Zhang and Henrich 1994).

Several articles reported the visible light emission of vanadium oxide supported on different metal oxides upon excitation (Anpo 1980; Patterson et al. 1991; Iwamoto et al. 1983; Garcia et al. 2000). It has been found that V = O vanadyl groups are the most active sites for the PL emission; the position of the emission band depends on the carriers and contents in various supported vanadium oxides (Iwamoto et al. 1983). The PL of V_2O_5 anchored on SiO_2 support indicates that phosphorescence takes place because of charge transfer process on the surface vanadyl groups. It involves an electron transfer from O^{2-} to V^{5+} ions, which results in the formation of pairs of hole centres (O^-) and trapped electrons (V^{4+}) as well as a reverse radiative decay by disappearance of hole–electron pair (Patterson et al. 1991). Frank–Condon analysis indicates that the inter-nuclear equilibrium distance between the vanadium and oxygen ions during the charge transfer process in excited state is larger by 0.012 nm than that in its ground state. This change in the inter-nuclear distance between the two states allows the transitions to a number of excited vibrational levels according to Frank–Condon principle. The PL spectrum obtained from V_2O_5 supported on porous vycor glass (PVG) further confirms that the energy band separation in the vibrational fine structure corresponds to the vibration energy of the double bond in the surface vanadyl groups, which becomes weak on excitation (Anpo 1980).

In another study, the solid–state reaction has been investigated between zeolite and V_2O_5 (Zhang et al. 1998). The PL with the strong peak at 500 nm has been reported with the vibrational fine structure similar to that of the four-fold tetrahedrally coordinated V^{5+} species, which have V = O vanadyl groups and were highly dispersed on SiO_2.

The crystal structure of $Zn_3(VO_4)_2$ consists of octahedral Zn ions connected by vanadate groups. The VO_4^{3-} anion group is tetrahedral and four O^{2-} ions are bounded by covalent bonds to the central V^{5+} metal ion. Luminescence phenomenon reported for other vanadate complexes such as $Mg_3(VO_4)_2$, $LiZnVO_4$, and $NaCaVO_4$ also involves one-electron charge transfer process from the oxygen 2*p* orbital to the 3*d* orbital of the V^{5+} ion. Considering the electronic structure of VO_4^{3-} ion in T_d symmetry, the bluish-green luminescence of the vanadate group in $Ba_3V_2O_8$ has been observed due to both $^3T_2 \rightarrow {}^1A_1$ transition for λ_{max} = 490 nm and the $^3T_1 \rightarrow {}^1A_1$ transition for λ_{max} = 525 nm (Park and Mho 2007). Red emission has been reported by the Eu^{3+}-activated $Ca_3Sr_3(VO_4)_4$ complex at 618 nm because of non-radiative transfer of absorbed photons by VO_4^{3-} groups inside the host matrix to the luminescent centres like Eu^{3+} (Choi et al. 2009). According to the above reports and the results obtained here, we can deduce that the origin of high PL in the $Zn_3(VO_4)_2$ is due to the charge transfer transitions of VO_4^{3-} group, and it can act as an efficient self-activated phosphor material.

Conclusions

Two types of samples have been prepared by DC magnetron sputtering of ZnO and V_2O_5 targets and subsequent annealing in oxygen atmosphere. Sample A was prepared by dual-target co-sputtering of ZnO and V_2O_5, whereas sample B was formed by deposition of V_2O_5 and ZnO thin layers with separate, independent steps. SEM and XRD results have shown the formation of crystalline α-$Zn_3(VO_4)_2$ on post heat treatment at 500 °C. The un-annealed samples do not show $Zn_3(VO_4)_2$ compound, which confirms that V_2O_5 and ZnO can only form a solid solution at a critical annealing temperature. The atomic ratio of Zn:V:O is in good agreement with the molecular formula of $Zn_3(VO_4)_2$ in the sample B, while the sample A has shown more Zn interstitials and oxygen vacancies because of the nonuniform distribution of Zn, V and O atoms from the dual-target co-sputtering.

PL measurements at room temperature exhibit a weak UV emission band from ZnO and strong emission band in the visible region from $Zn_3(VO_4)_2$. It is observed that the presence of Zn interstitials and oxygen vacancies decreases the photoemission in the visible region. Based on the charge transfer and Frank–Condon principle, we propose that the $(VO_4)^{3-}$ ions should be the luminescent centres for the visible light emission from $Zn_3(VO_4)_2$. By optimizing the deposition parameters, PL intensity is expected to be improved further, which demonstrates that the $Zn_3(VO_4)_2$ compound should be a promising material for light emission applications.

Acknowledgments The authors are grateful to Mrs. Catherine Hobbis and Dr. Alec Asadov for their technical assistance. One of the authors is supported by Pakistan HEC Ph.D. Scholarship. The authors also acknowledge the supports from the University of Science and Technology China for the photoluminescence measurements.

References

Anpo M (1980) Photoluminescence and photoreduction of V_2O_5 supported on porous vycor glass. J Phys Chem 84(25):3440–3443

Chen XY, Ng AMC, Fang F, Djurisic AB, Chan WK, Tam HL, Cheah KW, Fong PWK, Lui HF, Surya C (2010) The influence of the ZnO seed layer on the ZnO nanorod/GaN LEDs. J Electrochem Soc 157(3):H308–H311

Choi S, Moon Y-M, Kim K, Jung H-K, Nahm S (2009) Luminescent properties of a novel red-emitting phosphor: Eu^{3+}-activated $Ca_3Sr_3(VO_4)_4$. J Lumin 129(9):988–990

Fei H-L, Zhou H-J, Wang J-G, Sun P-C, Ding D-T, Chen T-H (2008) Synthesis of hollow V_2O_5 microspheres and application to photocatalysis. Solid State Sci 10(10):1276–1284. doi: 10.1016/j.solidstatesciences.2007.12.026

Filonenko VP, Sundberg M, Werner PE, Zibrov IP (2004) Structure of a high-pressure phase of vanadium pentoxide beta-V_2O_5. Acta Crystallogr Sect B-Struct Sci 60:375–381

Garcia H, Nieto JML, Palomares E, Solsona B (2000) Photoluminescence of supported vanadia catalysts: linear correlation between the vanadyl emission wavelength and the isoelectric point of the oxide support. Catal Lett 69(3–4):217–221

Hng HH, Knowles KM (1999) Characterisation of $Zn_3(VO_4)_2$ phases in V_2O_5 doped ZnO varistors. J Eur Ceram Soc 19(6–7):721–726

Hoyos DA, Echavarria A, Saldarriaga C (2001) Synthesis and structure of a porous zinc vanadate, $Zn_3(VO_4)_2{\cdot}3H_2O$. J Mater Sci 36(22):5515–5518

Hu RR, Zhong SH (2005) Mutual modification V_2O_5 and TiO_2 on the surface of supported coupled-semiconductor V_2O_5-TiO_2/SiO_2. Chin J Catal 26(1):32–36

Iwamoto M, Furukawa H, Matsukami K, Takenaka T, Kagawa S (1983) Diffuse reflectance infrared and photoluminescence spectra of surface vanadyl groups. Direct evidence for change of bond strength and electronic structure of metal-oxygen bond upon supporting oxide. J Am Chem Soc 105(11):3719–3720

Khyzhun OY, Strunskus T, Grünert W, Woll C (2005) Valence band electronic structure of V_2O_5 as determined by resonant soft X-ray emission spectroscopy. J Electron Spectrosc Relat Phenom 149(1–3):45–50

Kim JJ, Hur TB, Sung KJ, Kywon DY (2005) Solubility of V_2O_5 in polycrystalline ZnO with different sintering conditions. J Korean Phys Soc 47:333–335

Krithiga R, Chandrasekaran G (2009) Synthesis, structural and optical properties of vanadium doped zinc oxide nanograins. J Cryst Growth 311(21):4610–4614

Kurzawa M, Rychlowska-Himmel I, Bosacka M, Blonska-Tabero A (2001) Reinvestigation of phase equilibria in the V_2O_5–ZnO system. J Therm Anal Calorim 64(3):1113–1119

Legrouri A (1993) Electron optical studies of fresh and reduced vanadium pentoxide-supported rhodium catalysts. J Catal 140(1):173–183

Liu J, Yang R, Li S (2007) Synthesis and photocatalytic activity of TiO_2/V_2O_5 composite catalyst doped with rare earth ions. J Rare Earths 25(2):173–178

Moshfegh AZ (1991) Formation and characterization of thin film vanadium oxides: Auger electron spectroscopy, X-ray photoelectron spectroscopy, X-ray diffraction, scanning electron microscopy, and optical reflectance studies. Thin Solid Films 198(1–2):251–268

Muller S, Lorenz M, Czekalla C, Benndorf G, Hochmuth H, Grundmann M, Schmidt H, Ronning C (2008) Intense white photoluminescence emission of V-implanted zinc oxide thin films-art. no. 123504. J Appl Phys 104(12):123504

Ni S, Wang X, Zhou G, Yang F, Wang J, He D (2010) Crystallized $Zn_3(VO_4)_2$: synthesis, characterization and optical property. J Alloy Compd 491(1–2):378–381

Park KC, Mho Si (2007) Photoluminescence properties of $Ba_3V_2O_8$, $Ba_{3(1-x)}Eu_{2x}V_2O_8$ and $Ba_2Y_2/3V_2O_8$:Eu^{3+}. J Lumin 122–123 (1–2):95–98

Patterson HH, Cheng J, Despres S, Sunamoto M, Anpo M (1991) Relationship between the geometry of the excited state of vanadium oxides anchored onto SiO_2 and their photoreactivity toward CO molecules. J Phys Chem 95(22):8813–8818

Pitale SS, Gohain M, Nagpure IM, Ntwaeaborwa OM, Bezuidenhoudt BCB, Swart HC (2012) A comparative study on structural, morphological and luminescence characteristics of $Zn_3(VO_4)_2$

phosphor prepared via hydrothermal and citrate-gel combustion routes. Physica B 407(10):1485–1488

Schoiswohl J, Kresse G, Surnev S, Sock M, Ramsey MG, Netzer FP (2004) Planar vanadium oxide clusters: Two-dimensional evaporation and diffusion on Rh(111). Phys Rev Lett 92(20):206101–206103

Stoyanov S, Mladenova D, Dushkin C (2006) Photocatalytic properties of mixed TiO_2/V_2O_5 films in water purification at varying pH. React Kinet Catal Lett 88(2):277–283. doi:10.1007/s11144-006-0062-y

Talledo A, Valdivia H, Benndorf C (2003) Investigation of oxide (V_2O_5) thin films as electrodes for rechargeable microbatteries using Li. J Vac Sci Technol Vac Surf Films 21(4):1494–1499

Umemura R, Ogawa H, Kan A (2006) Low temperature sintering and microwave dielectric properties of $(Mg_{3-x}Zn_x)(VO_4)_2$ ceramics. J Eur Ceram Soc 26(10–11):2063–2068

Wang Y, Li Z, Sheng X, Zhang Z (2007) Synthesis and optical properties of V_2O_5 nanorods. J Chem Phys 126(16):164701

Wang L, Xu Z, Zhao S, Lu L, Zhang F (2010) Effect of vanadium content on photoluminescence and magnetic properties of doped ZnO thin films. Mod Phys Lett B 24(10):945–951

Zhang Z, Henrich VE (1994) Surface electronic structure of $V_2O_5(001)$: defect states and chemisorption. Surf Sci 321(1–2):133–144

Zhang SG, Higashimoto Hiromi Y, Masakazu A (1998) Characterization of vanadium oxide/ZSM-5 zeolite catalysts prepared by the solid-state reaction and their photocatalytic reactivity: in situ photoluminescence, XAFS, ESR, FT-IR, and UV–Vis investigations. J Phys Chem B 102:5590–5594

Zou CW, Yan XD, Han J, Chen RQ, Gao W (2009a) Microstructures and optical properties of β-V_2O_5 nanorods prepared by magnetron sputtering. J Phys D Appl Phys 42(14):145402

Zou CW, Yan XD, Patterson DA, Emanuelsson EAC, Bian JM, Gao W (2009b) Temperature sensitive crystallization of V_2O_5: from amorphous film to β-V_2O_5 nanorods. CrystEngComm 12(3):691–693

Zou CW, Rao YF, Alyamani A, Chu W, Chen MJ, Patterson DA, Emanuelsson EAC, Gao W (2010a) Heterogeneous lollipop-like V_2O_5/ZnO array: a promising composite nanostructure for visible light photocatalysis. Langmuir 26(14):11615–11620

Zou CW, Yan XD, Bian JM, Gao W (2010b) Enhanced visible photoluminescence of V_2O_5 via coupling ZnO/V_2O_5 composite nanostructures. Opt Lett 35(8):1145–1147